Enhanced Electron Mobility Due to Dopant-Defect Pairing in Conductive ZnMgO

*Yi Ke, Stephan Lany, Joseph J. Berry, John D. Perkins, Philip A. Parilla, Andriy Zakutayev, Tim Ohno, Ryan O'Hayre, and David S. Ginley**

The increase of the band gap in $Zn_{1-x}Mg_xO$ alloys with added Mg facilitates tunable control of the conduction band alignment and the Fermi-level position in oxide-heterostructures. However, the maximal conductivity achievable by doping decreases considerably at higher Mg compositions, which limits practical application as a wide-gap transparent conductive oxide. In this work, first-principles calculations and material synthesis and characterization are combined to show that the leading cause of the conductivity decrease is the increased formation of acceptor-like compensating intrinsic defects, such as zinc vacancies (V_{Zn}), which reduce the free electron concentration and decrease the mobility through ionized impurity scattering. Following the expectation that non-equilibrium deposition techniques should create a more random distribution of oppositely charged dopants and defects compared to the thermodynamic limit, the paring between dopant Ga_{Zn} and intrinsic defects V_{Zn} is studied as a means to reduce the ionized impurity scattering. Indeed, the post-deposition annealing of Ga-doped $Zn_{0.7}Mg_{0.3}O$ films grown by pulsed laser deposition increases the mobility by 50% resulting in a conductivity as high as $\sigma = 475$ S cm^{-1}.

1. Introduction

Alloying Mg into ZnO increases the room-temperature band gap energy from ≈3.3 eV for ZnO to ≈3.8 eV for $Zn_{0.7}Mg_{0.3}O$.[1] Also, like ZnO itself, Zn(Mg)O can be degenerately doped n-type by substitutional doping on the cation lattice with Al, Ga or In.[2–4] Accordingly, Mg-substituted ZnO ($Zn_{1-x}Mg_xO$) is a candidate band-gap-energy tunable and band-edge-energy tunable transparent conducting oxide (TCO). This tunability is of great use in optimizing the performance of many opto-electonic devices.[5–12] However, a substantial and usually undesired decrease in the maximum obtainable conductivity is observed with increasing Mg content.[2–4,13–16] For thin films grown by physical vapor deposition methods, $Zn_{1-x}Mg_xO$ retains the ZnO wurtzite structure for Mg content up to $x \approx 0.35$.[1,14] Across this compositional range, the highest conductivities (σ) reported for doped Zn(Mg)O epitaxial films on single crystal sapphire substrates decrease from $\sigma \approx 10\,000$ S cm^{-1} for $x = 0$ [17–19] to $\sigma \approx 1500$ S cm^{-1} for $x = 0.1$[2,13,14] to $\sigma \approx 300$ S cm^{-1} for $x = 0.3$.[2,13,14] Hall-effect measurements show that decreases in both the free carrier concentration (n) and the electron mobility (μ) contribute to the decrease in conductivity.[2,14] For example, in our prior work on 1% Ga-doped Zn(Mg)O, n decreased by a factor of 2 and μ decreased by a factor of 2.5 yielding a five-fold reduction in the conductivity as the Mg content increased from $x = 0.1$ to 0.3.[14]

While the reduction of conductivity in ZnMgO alloys is widely observed,[2–4,13–16] there is no consensus as to the fundamental cause. For the decrease in the free carrier concentration, both an increasing donor activation energy due to either a larger effective mass[2,16,20] or change of band structure,[21] and a lowering of the active donor concentration due to composition enrichment[2,22] have been suggested. There is also a substantial decrease in the mobility from $\mu \approx 48$ cm^2 V^{-1} s^{-1} for Al-doped ZnO[17] to $\mu \approx 9$ cm^2 V^{-1} s^{-1} for Ga-doped $Zn_{0.7}Mg_{0.3}O$ films.[14] Even when a fairly large increase of the effective mass from 0.3 m_e in ZnO to ≈0.6 m_e in $Zn_{0.7}Mg_{0.3}O$[20] is assumed, an additional reduction by a factor of 2.5 needs to be accounted for, and has been variously attributed to increased alloy scattering,[3,23] increasing impurity scattering,[2] and enhanced grain boundary scattering due to fewer carriers.[4]

Using combined material synthesis, electrical transport measurements and first-principles theory, we here demonstrate that the reduction in conductivity in high quality epitaxial Ga-doped $Zn_{0.7}Mg_{0.3}O$ thin films is dominated by an increased self-compensation and reduced doping efficiency compared to ZnO. However, the formation of intrinsic compensating acceptors, generally attributed to Zn vacancies V_{Zn},[24–29] leads not only to a reduction of the doping efficiency, but also to a reduced mobility due to the additional ionized impurity scattering centers. Given that a higher degree of self-compensation

Y. Ke, S. Lany, J. J. Berry, J. D. Perkins, P. A. Parilla, A. Zakutayev, D. S. Ginley
National Renewable Energy Laboratory
Golden, CO 80401, USA
E-mail: David.Ginley@nrel.gov
Y. Ke, R. O'Hayre
Colorado School of Mines
Department of Metallurgical and Materials Engineering
Golden, CO 80401, USA
T. Ohno
Colorado School of Mines
Department of Physics
Golden, CO 80401, USA

DOI: 10.1002/adfm.201303204

Table 1. The band gap, effective electron mass, and dielectric constant of ZnO and the linear variation (d/dx) thereof with the Mg composition x. The computational results (theory) or the present work are compared with experimental literature data.

	ZnO E_g [eV]	d/dx E_g [eV]	ZnO m^*/m_e	d/dx m^*/m_e	ZnO $\varepsilon/\varepsilon_0$	d/dx $\varepsilon/\varepsilon_0$
Theory[a)]	3.31	2.0	0.39	0.22	7.39	–3.2
Experimental data	3.32[36]	2.27[37]	0.27[38]	0.90[20]	8.15[39]	–1.8[31]

[a)]Calculation results from this work.

is difficult to avoid in wider gap ZnMgO alloys, we study here the possibility of reducing the total scattering centers by pairing charged dopants and defects to form defect pairs and complexes in lower charge states. The observed 50% increase in mobility upon annealing for Ga-doped $Zn_{0.7}Mg_{0.3}O$ thin films is attributed to such defect pairing. Further, this dopant-defect pairing strategy should be applicable to other wide-band-gap semiconductors as well, in particular when non-equilibrium growth causes a more random distribution of charged defect centers than expected for equilibrium growth.

2. Donor Levels in ZnMgO Alloys (Theory)

We first investigate theoretically whether the composition dependence of the donor ionization energies affects the electrical properties of ZnMgO alloys. Particularly, the donor ionization energy of Al, Ga, and In, the common group III dopants in ZnO and ZnMgO, are calculated both via the well-established effective-mass approximation (EMA) and supercell approach (SCA).[30] Within the EMA, the ionization energy depends only on the effective mass m^* of the majority charge carriers (here, electrons) and the dielectric constant ε.

$$E_d = \frac{13.6\ eV \cdot m^*/m_e}{(\varepsilon/\varepsilon_0)^2} \quad (1)$$

Notably, these parameters are properties of the semiconductor host materials, and are independent of the chemical species used for doping (e.g., Al, Ga, In in ZnO). The EMA holds for shallow, hydrogenic donor levels, but breaks down when the defect state becomes deep and localized. In this case, the SCA is more appropriate for the prediction of the donor ionization energy.

The materials parameters m^* and ε, which determine the donor ionization energy in the EMA, are well established for ZnO, and recent experiments have examined their composition dependence in ZnMgO alloys.[20,31] The theoretical prediction of the band-structure properties of such alloys is challenging, because accurate GW quasiparticle energy calculations[32,33] are computationally demanding, limiting their application presently to crystal structures with relatively small unit cells. Therefore, we employ here a density functional theory (DFT) based approach with empirical on-site potentials,[34] which avoids the common band gap problem of standard local density calculations. The empirical potential terms are fitted to GW reference calculations for pure ZnO and MgO (see also Computational Methods section below). Using this method, we performed calculations of random alloy configurations in 192 atom supercells, thereby obtaining the approximate predictions for the composition dependence of the band gap E_g, the effective mass m^*, and the dielectric constant ε. In a related theoretical work,[35] the alloy problem was addressed instead by a cluster expansion approach for the calculation of configurational averages. However, our approach here also enables the self-consistent band gap corrected calculations of defects in the SCA (see below).

The composition dependence of the band gap energy is usually expressed up to quadratic order,

$$E_g(x) = (1-x)\cdot E_g^{ZnO} + x\cdot E_g^{MgO\text{-}wz} + b\cdot x(1-x) \quad (2)$$

where our calculations give the band gap of ZnO as E_g^{ZnO} = 3.31 eV, and the band gap of the hypothetical MgO wurtzite phase as $E_g^{MgO\text{-}wz}$ = 5.65 eV. The bowing parameter b = 0.07 eV is very small, indicating essentially a linear variation of E_g with composition. The values of E_g, m^*, and ε for ZnO, as well as their linear variation with the Mg composition x are given in **Table 1** along with a list of experimental data from the literature for comparison. When using the theory data in Table 1 to calculate the donor ionization energy E_i of ZnO in the EMA (Equation 1), we obtain 97 meV. This result is somewhat larger than the expected value of 55 meV based on the experimentally determined materials parameters. This discrepancy is due to an overestimated effective mass and an underestimation of the dielectric constant (Table 1). Despite the quantitative difference due to the sensitivity of the EMA energy on the materials parameters (note the reciprocal quadratic dependence on ε in Equation 1), we expect that the calculations should still effectively capture the qualitative trends and relative changes with composition. Specifically, we predict that at the composition x = 0.3 used for the experimental film fabrication in this work, the ionization energy E_i^{EMA} is increased by about 50%.

In order to address the question whether the common group III dopants in ZnO and ZnMgO, that is, Al, Ga, and In, remain effective-mass-like donors with increasing Mg composition, we calculated the donor ionization energies also in the SCA. We find that for Al and Ga the SCA does not predict a significant increase of the donor binding energy over the EMA, suggesting that these dopants act like hydrogenic donors in $Zn_{1-x}Mg_xO$ alloys over the entire studied composition range up to x = 0.5. However, In donors exhibit a pronounced deep level character for Mg compositions above $x \geq 0.4$. The calculated donor levels for these dopants as a function of x is shown in **Figure 1** relative to the conduction band minimum (CBM) and valence band maximum (VBM).

An inspection of the character of the wave function for the In case suggests that the In-5s orbital hybridizes with the CBM

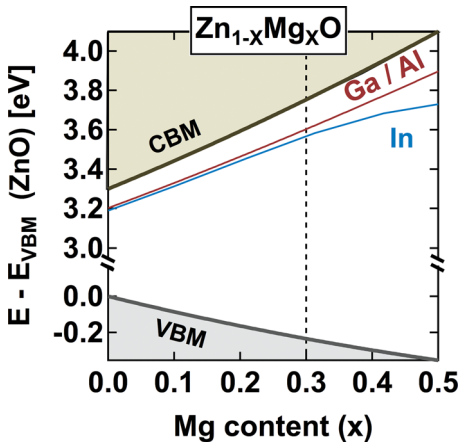

Figure 1. The variation of the band gap energy with composition in $Zn_{1-x}Mg_xO$ alloys, obtained in a self-consistent band-gap corrected DFT calculation employing empirical on-site potentials, showing also the donor levels for Al, Ga, and In.

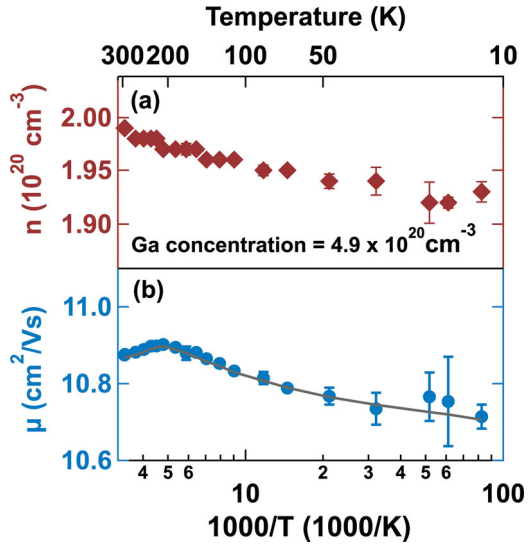

Figure 2. Temperature dependent Hall effect measurements showing a) carrier concentration and b) mobility for $Zn_{0.7}Mg_{0.29}Ga_{0.01}O$.

to form a donor state with a large central-cell contribution[40] that enhances the localization at the In site. For the case of the Al and Ga donors, which have spatially less extended *s*-orbitals, this hybridization is negligible, and so they retain their effective-mass-like donor character. Notably, this trend is also reflected in the slight variation of the experimental ionization energies for Al, Ga, and In in pure ZnO, which have been measured by photoluminescence to be 53, 54.5, and 63.2 meV, respectively.[41] The results of the calculations then indicate that there is only a modest effect on the electrical properties due to the gradual increase of the effective hydrogenic binding energy, except for the case of In, where a considerable increase of ionization energy at high Mg composition could limit the conductivity more severely.

3. Electrical Properties (Experiment)

The samples for the experimental studies were epitaxial $Zn_{0.7}Mg_{0.29}Ga_{0.01}O$ thin films deposited from solid oxide targets by pulsed laser deposition on single crystal c-plane sapphire substrates at a temperature of 400 °C. The chamber atmosphere for the depositions was 1×10^{-5} Torr O_2 and 1×10^{-3} Torr Ar with anneals performed at 400 °C in a $pO_2 = 10^{-7}$ Torr atmosphere. In preliminary experiments (not shown), the oxygen partial pressure during growth was varied over the range $10^{-7} < pO_2 < 10^{-2}$ Torr. For $pO_2 > 10^{-4}$ Torr, the room temperature carrier concentration (n) and conductivity (σ) increase rapidly with decreasing pO_2. For the $pO_2 < 10^{-4}$ Torr, the conductivity, carrier concentration and mobility (μ) are all nearly constant. Accordingly, samples grown at $pO_2 = 10^{-5}$ Torr are taken to be representative of these higher conductivity $Zn_{0.7}Mg_{0.29}Ga_{0.01}O$ films. Additional details are provided in the methodology section.

The carrier concentration and mobility measured by Hall effect as a function of measurement temperature (T) are shown in **Figure 2**. First, we note that the carrier concentration is essentially temperature independent, varying less than 5% over the temperature range $10 < T < 300$ K. An Arrhenius analysis of the slight increase observed with increasing temperature yields an activation-energy of less than 1 meV, much less than the expected 55 meV binding energy for a simply hydrogenic donor in $Zn_{0.7}Mg_{0.3}O$. This observation, combined with the high measured carrier concentration, $n \approx 2 \times 10^{20}$ cm^{-3} indicates that Ga is indeed a shallow dopant in $Zn_{0.7}Mg_{0.3}O$ and that the resulting samples are degenerately doped.

Despite the small ionization energy of the Ga dopant, the measured doping efficiency is rather low. Specifically, the carrier concentration is only 40% of the Ga concentration, which was independently measured in the deposited films by both ICP and XRF and determined to be 1.1 at% ($N_{Ga} = 4.9 \times 10^{20}$ cm^{-3}). ICP, XRF, and EDX compositional analyses do not indicate any impurities besides Ga with concentrations larger than 10^{20} cm^{-3} in the deposited films. Thus, the potential presence of unintended extrinsic compensating acceptors at the level needed to account for the observed doping efficiency is excluded. Another possible cause for the low doping efficiency is extended defects (e.g., second phase inclusions, grain boundaries), but structural measurements on these films suggest that this is not the case. Specifically, characterization of the films using XRD pole figure, HRTEM, and Selected Area Diffraction Pattern (SADP) show that the films are highly epitaxial and have no sign of secondary crystalline or amorphous phases. Furthermore, atomic-resolution EDX scans show that the Zn and Mg atoms are distributed homogeneously throughout the films.

Another important mechanism that could lead to deterioration of the doping efficiency with increasing Mg composition is the formation of compensating defects. There is a growing body of evidence that Zn vacancies are the dominant compensating acceptors in n-type ZnO, even when grown in oxygen-poor atmospheres chosen to promote high carrier concentration. Theory predicts a low formation energy for charged V_{Zn}^{2-} defects when the Fermi level rises close to the conduction band in n-type ZnO.[24–26] Despite the challenge to directly measure point defect distributions, strong experimental

evidence for V_{Zn} as the main acceptors in n-type ZnO have been reported, including positron annihilation and luminescence measurements.[27,28] In ZnMgO alloys, the increase of the band gap with Mg composition is mostly due to an increase of the CBM energy, according to our results shown in Figure 1. Note that the change of the band edge energies with Mg composition is given with respect to the average electrostatic potential of ZnO, which is a suitable reference for the formation energy of charged defects.[42] The increase of the CBM energy is expected to further lower the formation energy of charged V_{Zn}^{2-} defects, as the Fermi energy increases accordingly for a given electron concentration. Although the concentration of compensating defects can be far away from those described by the defect-equilibrium,[43] it can nevertheless be expected that V_{Zn} defects will form more easily with increasing Mg composition, compensating the free electrons and acting as ionized impurity scattering centers.

4. Defect Model for Charged Impurity Scattering

Figure 2b shows the change of Hall mobility as a function of temperature. The mobility increases slowly with temperature from 10 K to 250 K then slightly decreases with a further increase in temperature. However, the total variation of mobility within the 10 K to 300 K temperature range is only ≈2%. Accordingly, the major scattering mechanism must be temperature-independent and the electron transport only slightly influenced by other secondary temperature dependent scattering mechanisms. To quantify this, we have fit the temperature dependence of the measured Hall mobility including contributions from different candidate scattering mechanisms. The results of this analysis are shown in **Figure 3**. The major scattering mechanism is ionized impurities (μ_{ii}) with the next strongest scattering processes being optical phonon scattering (μ_{pop}) and thermionic emission at the grain boundaries (μ_{bdry}) depending on the temperature. Scattering due to acoustic phonon scattering (μ_{ac}) and piezoelectric phonon scattering (μ_{pie}) are weaker still. Similar results have been widely found in heavily doped ZnO and further details are provided in the Supporting Information.

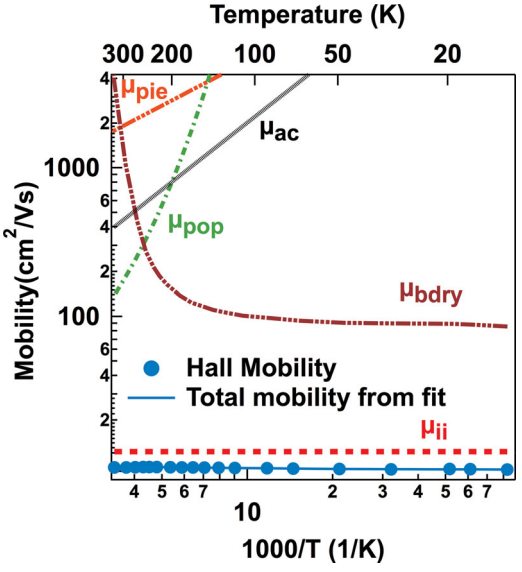

Figure 3. Analysis of the temperature-dependent mobility to examine the scattering mechanisms that contribute to the as-measured Hall mobility from Figure 2b (filled circles), broken down into different scattering mechanisms. The best fit is obtained for an ionized scattering center concentration $N_{ii} = 6.7 \times 10^{20}$ cm^{-3}.

We also considered alloy scattering, which has previously been used to explain the additional scattering in Al-doped $Zn_{0.88}Mg_{0.12}O$ thin films.[23] A strict application of the same alloy scattering formalism[44] but with material parameters appropriate for $Zn_{0.7}Mg_{0.3}O$ suggests that alloy scattering would be the next most significant scattering process after ionized impurity scattering with $\mu_{alloy} \approx 30$ cm^2 V^{-1} s^{-1} at $T = 300$ K. However, this model is intended for nearly intrinsic semiconductors, not degenerately doped materials where there is substantial screening due to free carriers. Further, $\mu_{alloy} \propto T^{-1/2}$ which would result in a temperature dependence both opposite in sign and 25 times larger than the one observed (see Figure 2b). As a result, we believe that any alloy scattering present must be small compared to the temperature independent ionized impurity scattering.

Based on this analysis of the transport data we conclude that temperature-independent ionized impurity scattering is by far the dominant effect limiting the electron mobility. Hence, from here forward, we focus on better understating the possible sources of ionized impurity scattering in Ga-doped $Zn_{0.7}Mg_{0.3}O$ and how, if at all, this scattering might be reduced. Accordingly, we adopted the formalism of Look et al.[28] for modeling self-compensation in degenerate semiconductors. We assume that Ga donors are the only dopants and exist as fully ionized Ga_{Zn}^{+} defects. Therefore, the ionized impurity scattering can be calculated by the Brooks-Herring (B-H) theory as

$$\mu_{ii}(n, n_{ii}) = \mu_{ii0}(n) n / Z^2 n_{ii} \tag{3}$$

where n_{ii} is the concentration of ionized impurities of charge Z, n the charged carrier concentration, and $\mu_{ii0}(n)$ is given by

$$\mu_{ii0}(n) = \frac{24\pi^3 \varepsilon_0^2 \hbar^3}{e^3 m^{*2}} \frac{1}{\ln[1+\gamma(n)] - \frac{\gamma(n)}{1+\gamma(n)}} \tag{4}$$

where

$$\gamma(n) = \frac{3^{1/3} 4\pi^{8/3} \varepsilon_0 \hbar^2 n^{1/3}}{e^2 m^*} \tag{5}$$

In the case of multiple types of scattering centers, Equation 3 can be generalized by implementing Matthiessen's rule:

$$\mu_{ii}^{-1}(n) = \mu_{ii0}(n)^{-1} \frac{\sum Z_{Dj}^2 N_{Dj} + \sum Z_{Aj}^2 N_{Aj}}{n} = \mu_{ii0}(n)^{-1} \frac{N_{ii}}{n} \tag{6}$$

According to literature, the static dielectric constant ε of $Zn_{0.7}Mg_{0.3}O$ is $7.2\varepsilon_0$[31] and the effective mass m^* of $Zn_{0.7}Mg_{0.3}O$ is $0.57\ m_0$.[20] Since μ_{ii} is approximately 12.2 cm^2 V^{-1} s^{-1} (Figure 3), N_{ii} can be calculated as 6.7×10^{20} cm^{-3}, which is much larger than the free carrier concentration (1.96×10^{20} cm^{-3}).

Thus, the mobility analysis independently confirms the existence of ionized defects other than Ga_{Zn}^{+}, which is consistent with the conclusion above that the low doping efficiency is caused by the formation of negatively-charged compensating V_{Zn}^{2-} defects.

Oppositely charged defects tend to form pairs and complexes,[45] thereby changing the charge and the number of ionized impurities. In particular, the complex formation between group III donors and cation vacancies in n-doped II-VI semiconductors has been confirmed via measurements[46] and calculation[47] of hyperfine interaction parameters. Thus, in addition to the intentional Ga_{Zn}^{+} dopant and the compensating V_{Zn}^{2-} defect, we have to consider the singly charged $(Ga_{Zn} - V_{Zn})^{-}$ and the charge-neutral $(2Ga_{Zn} - V_{Zn})^{0}$ defect clusters.[26,28,29] In order to determine the expected relative abundance of the charged scattering centers, we next calculate their thermodynamic equilibrium concentration as a function of temperature. The binding energies of the $(Ga_{Zn} - V_{Zn})^{-}$ and $(2Ga_{Zn} - V_{Zn})^{0}$ complexes in $Zn_{0.7}Mg_{0.3}O$ are assumed to be the same as in ZnO, which were calculated in a DFT supercell approach to be $E_{b1} = -1.1$ eV and $E_{b2} = -1.8$ eV, respectively, relative to the isolated defect species.[43] The total Ga_{Zn} concentration N_{Ga}^{Tot} is taken to be the measured Ga concentration ($N_{Ga}^{Tot} = 4.9 \times 10^{20}$ cm^{-3}), and since each V_{Zn} defect compensates two Ga dopants (irrespective of the isolated or defect pair configuration), the total zinc vacancy concentration N_V^{Tot} is determined from the Ga concentration and the measured carrier concentration as $N_V^{Tot} = \frac{1}{2}(N_{Ga}^{Tot} - n)$. The defect cluster concentrations as a function of temperature are then calculated by applying the law of mass action.

$$N_{Ga\text{-}V} = N_{Ga} \times N_V \times \exp(-E_{b1}/kT) \quad (7)$$

$$N_{2Ga\text{-}V} = N_{Ga}^{2} \times N_V \times \exp(-E_{b2}/kT) \quad (8)$$

Here, N_{Ga}, N_V, are the concentrations of the isolated (unpaired) Ga_{Zn}^{+} dopants and V_{Zn}^{2-} defects, and $N_{Ga\text{-}V}$ and $N_{2Ga\text{-}V}$ are the concentrations of the $(Ga_{Zn} - V_{Zn})^{-}$ and $(2Ga_{Zn} - V_{Zn})^{0}$ complexes, respectively.

As seen in **Figure 4**, the large thermodynamic driving force for the Ga_{Zn} defects to pair with intrinsic V_{Zn} defects leads, in an equilibrium situation below 1000 °C, to a complete pairing of V_{Zn} defects. It is clear such equilibrium state also minimizes the ionized impurity scattering as reflected by the reduction of the N_{ii}, when considering the quadratic dependence of the scattering strength on the defect charge in Equation (6):

$$N_{ii} = N_{Ga} + N_{Ga\text{-}V} + 4N_V \quad (9)$$

According to above analysis, if the dopant-defect pair association would equilibrate in the films examined in Figure 2 at the growth temperature of 400 °C, most V_{Zn}^{2-} scattering centers would become bound in charge-neutral $(2Ga_{Zn} - V_{Zn})^{0}$ complexes, reducing N_{ii} essentially to the number of uncompensated Ga_{Zn} donors, that is, $N_{ii} = n = 2.0 \times 10^{20}$ cm^{-3}. This expected value is less than 1/3 of the effective number $N_{ii} = 6.7 \times 10^{20}$ cm^{-3} of scattering centers determined above from the electrical characterization. Such discrepancy suggests the defect distribution in actual thin film samples grown by non-equilibrium processes (such as PLD used here) is not fully equilibrated.

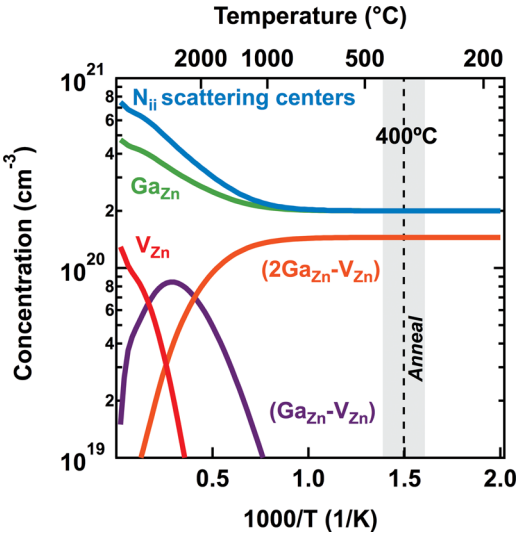

Figure 4. The temperature dependence of thermodynamic defect densities, calculated by applying the law of mass action to the carrier concentration (n) and Ga concentrations and taking into account the binding energies of the $(Ga_{Zn} - V_{Zn})^{-}$ and $(2Ga_{Zn} - V_{Zn})^{0}$ complexes.

In order to determine the individual concentrations of the different defect centers from the available experimental data, we assume that the concentration of the fully passivated $(2Ga_{Zn} - V_{Zn})^{0}$ complex is small in the as-grown films. This assumption is justified by the fact that the direct formation of this three-defect complex is statistically rather unlikely, as its formation requires diffusion of the Ga impurities. However, since cation diffusion occurs via a vacancy mechanism,[48,49] the Ga diffusion should be slower than the self-diffusion (i.e., the V_{Zn} diffusion) due to the small impurity to host–cation ratio. Thus, we can initially reduce the types of defect centers to three, that is, Ga_{Zn}^{+}, V_{Zn}^{-2} and $(Ga_{Zn} - V_{Zn})^{-}$, which allows calculating the individual concentrations of these centers as follows.

First, we can feed $N_{ii} = 6.7 \times 10^{20}$ cm^{-3}, calculated from mobility analysis, into Equation (9) to obtain one relationship. In addition, considering the charge neutrality condition and the conservation of Ga atoms yields two additional relationships,

$$n = N_{Ga} - N_{Ga\text{-}V} - 2N_V, \text{ and} \quad (10)$$

$$N_{Ga}^{Tot} = N_{Ga} + N_{Ga\text{-}V} \quad (11)$$

where $n = 1.96 \times 10^{20}$ cm^{-3} and $N_{Ga}^{Tot} = 4.9 \times 10^{20}$ cm^{-3} as determined above. Solving Equations (9)–(11) for N_V, $N_{Ga\text{-}V}$, and N_{Ga} yields $N_V = 4.5 \times 10^{19}$ cm^{-3}, $N_{Ga\text{-}V} = 1.0 \times 10^{20}$ cm^{-3}, $N_{Ga} = 3.9 \times 10^{20}$ cm^{-3}. These are physically reasonable values, comparable with the values previously reported for degenerate ZnO,[28] and they consistently explain within the ionized impurity scattering model the quantitative values of the measured mobility and carrier concentration.

By comparison, the concentrations N_V and $N_{Ga\text{-}V}$ of the charged centers, determined by this modeling, are much higher than expected for thermodynamic equilibrium (Figure 4) at the growth temperature $T = 400$ °C, where virtually all V_{Zn} defects

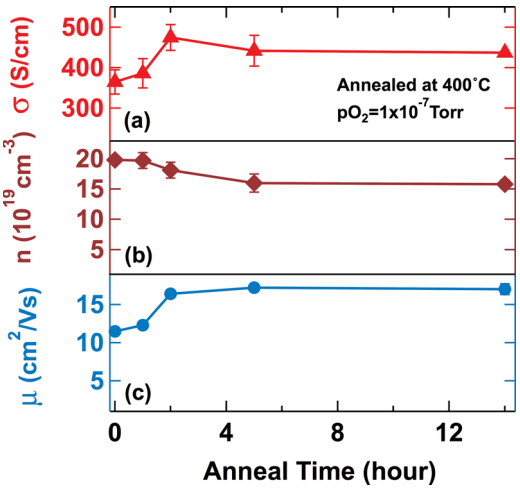

Figure 5. The change of a) conductivity, b) carrier concentration, and c) mobility during anneal.

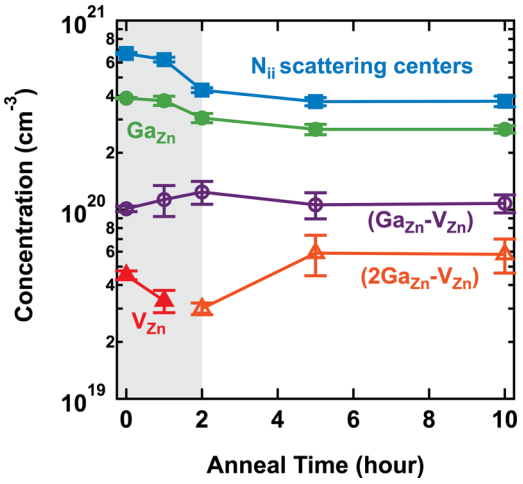

Figure 6. The change in defect densities during annealing based on fitting a Brooks-Herring model to the measured carrier concentration (n) and mobility (μ) from Figure 5. N_{ii} is the effective density of singly-charged scattering centers. Open symbols denote coupled defect complexes.

ought to be bound in charge neutral $(2Ga_{Zn} - V_{Zn})^0$ complexes. As a result, there are more scattering centers, that is, larger N_{ii}, in as-deposited films. This finding suggests that annealing should further promote the clustering of doubly charged isolated V_{Zn} defects into single charged $(Ga_{Zn} - V_{Zn})^-$ pairs and even into neutral $(2Ga_{Zn} - V_{Zn})^0$ clusters, reducing considerably the effective number N_{ii} of ionized impurity scattering centers and increasing the mobility.

5. Reduction of Scattering by Annealing

In order to test the possibility to reduce ionized impurity scattering by promoting the pairing of charged dopants and defects, a Ga-doped $Zn_{0.7}Mg_{0.3}O$ film, representative of our most conductive films, was sequentially annealed for a total of 14 hours at 400 °C (same as the deposition temperature) in vacuum with a measured residual $pO_2 = 10^{-7}$ Torr. The anneal was stopped at three intermediate times and the sample was removed for electrical characterization. No observable changes in thickness, composition, or crystal quality (FWHM of XRD peaks and grain size seen under TEM) occurred during the annealing.

The conductivity, carrier concentration and mobility as a function of anneal time are plotted in **Figure 5**. During the first 5 h of anneal, the carrier concentration reduces from 1.98×10^{20} cm^{-3} to 1.60×10^{20} cm^{-3} while mobility increases from 11.6 cm^2 V^{-1} s^{-1} to 17.2 cm^2 V^{-1} s^{-1}. After 5 h of annealing, the carrier concentration and mobility remain essentially constant. The maximum conductivity (σ = 475 S cm^{-1}) is obtained after 2 h of annealing. This is a 30% increase compared to the as-deposited sample and roughly a 50% increase compared to the highest conductivity obtained for as-deposited $Zn_{0.7}Mg_{0.3}O$ films in previous studies.[2,13,14] Further, the optical absorption onset of the films after annealing remains sharp and stays at 4.0 eV, indicating that the Mg stays in the wurtzite ZnMgO lattice.

Using the same approach adopted in Section 4 for the as-deposited samples, the defect populations in the annealed samples can be estimated from the carrier concentration and mobility data, assuming ionized impurity scattering limits the conductivity. They are plotted as a function of the annealing time in **Figure 6**. To avoid underdetermined fitting of the data, it is necessary to divide the annealing process into two stages. In the first stage ($t_{anneal} \leq 2$ h), the three variables are taken to be the same as in Section 4, that is, N_V, N_{Ga}, and $N_{Ga\text{-}V}$. The carrier concentration n and the mobility μ are taken from the measurement after each annealing step (cf. Figure 5), and N_{ii} is determined from the measured mobility based on Equation 6. During this first stage of annealing, the more mobile V_{Zn}^{2-} defects diffuse towards the Ga_{Zn}^+, forming additional $(Ga_{Zn} - V_{Zn})^-$ complexes. As above, the defect concentrations can be solved for using Equations 9–11. The fit of the data for t_{anneal} = 2 h yields $N_V = 0$ within the error margin, indicating that the isolated V_{Zn} vacancies are depleted due to the pairing process.

In the second stage ($t_{anneal} > 2$ h), when there are no more isolated V_{Zn} defects, the concentration of $(Ga_{Zn} - V_{Zn})^-$ complexes stabilizes and fully passivated $(2Ga_{Zn} - V_{Zn})^0$ complexes begin to form. The rate of this processes is kinetically slower compared to the formation of the $(Ga_{Zn} - V_{Zn})^-$ complexes associated with the first stage of the anneal as it requires diffusion of the Ga cations. Since $N_V = 0$ in the second stage, the fitting variables are now $N_{Ga,}N_{Ga\text{-}V,}$ and $N_{2Ga\text{-}V}$, and a system of three equations with three unknowns can again be established, similar to Equations 9–11:

$$N_{ii} = N_{Ga} + N_{Ga\text{-}V} \tag{12}$$

$$n = N_{Ga} - N_{Ga\text{-}V} - 2N_{2Ga\text{-}V} \tag{13}$$

$$N_{Ga}^{Tot} = N_{Ga} + N_{Ga\text{-}V} + 2N_{2Ga\text{-}V} \tag{14}$$

The individual defect concentrations associated with both stages of the annealing processes are shown in Figure 6 as a function of the annealing time. During the initial stage of annealing, the fairly rapid mobility changes are caused by the formation of the $(Ga_{Zn} - V_{Zn})^-$ complexes. Because the

diffusion of V_{Zn} towards the Ga_{Zn} species is facile, the population of $(Ga_{Zn} - V_{Zn})^-$ complexes equilibrates relatively quickly. Once all the V_{Zn} are fully associated in $(Ga_{Zn} - V_{Zn})^-$ complexes, further changes in mobility (stage 2) are more gradual as they depend on the much slower Ga diffusion process required to form $(2Ga_{Zn} - V_{Zn})^0$ complexes.

These basic findings on the dynamics of defect association during annealing should also be applicable to ZnO and explain the large variation in mobility for heavily doped ZnO.[50] In addition, the thermodynamically driven clustering of oppositely charged defects during annealing is consistent with the generally observed increase in mobility during annealing, even when there is no clear structural improvement and change in carrier concentration.[26,28,50,51] Based on these findings, we also suggest that suppressing the formation of intrinsic electron killers (e.g., during growth or subsequent post-processing) is critical to improve the conductivity in these materials. An effective strategy to realize reductions in these electron-killing complexes will enhance both carrier concentration and mobility in Ga-doped ZnMgO, resulting in improved conductivity. Practical approaches to address these mechanism may include annealing of films in the presence of Zn metal, such as has been recently done for Al-doped ZnO.[19]

6. Conclusions

This work demonstrates that Ga remains a shallow dopant in $Zn_{1-x}Mg_xO$ alloys at least up to 30% Mg composition. The doping efficiency is likely limited by self-compensation due to intrinsic V_{Zn} acceptors and its complexes. Our results suggest that ionized impurities are the dominant scattering centers in these Ga-doped $Zn_{0.7}Mg_{0.3}O$ films, similar to the situation in most degenerately doped ZnO films. However, the mobility in as-deposited $Zn_{0.7}Mg_{0.3}O$ is much lower than in ZnO due both to a larger effective mass and larger concentration of charged intrinsic acceptors. Post-deposition annealing yields a 50% increase in the mobility. Self-consistent modeling of the carrier and defect concentration and mobility suggest this change is due to dopant-defect complex formation, which reduces the net concentration of charged scattering centers. In order for the electrical transport properties of ZnMgO alloys to approach those of ZnO, synthesis strategies aimed at reducing the total zinc vacancy concentration will likely be necessary.

7. Experimental Section

Computational Details: The calculations of the composition dependence of the band gap, the conduction band effective mass, and the donor ionization energies were performed with the VASP code[52] using 192 atom supercells, projector augmented wave[53] potentials, and the generalized gradient approximation[54] with an energy cutoff of 320 eV. For the self-consistent band-gap corrected calculation, we used an extension of the non-local external potential method found elsewhere,[34] where we determined two parameters per atom type and angular momentum.[55] A dense $6 \times 6 \times 6$ k-point grid was used for the effective mass calculation. For the donor ionization energies we took into account the image charge corrections, potential alignment, and band filling effects.[56] The dielectric constant was calculated on smaller 16 atom cells of the ZnMgO alloy using a density functional perturbation theory approach.[57]

Film Deposition and Process: ZnMgO:Ga thin films were grown on 1 cm × 1 cm double-side polished single-crystal (0001) (c-plane) sapphire (α-Al_2O_3) substrates by pulsed laser deposition (PLD). A Lambda Physics Compex 201 KrF laser (248 nm wavelength, 25 ns pulse length, 5 Hz repetition rate) was used as the ablation source, with an output maintained at 244 mJ per pulse, resulting in an energy density of 1.3 J cm^{-2} over a 1.3 mm × 2 mm spot at the target surface for all depositions. A commercial 1-inch solid oxide $Zn_{0.79}Mg_{0.2}Ga_{0.01}O$ target was used, and the target-substrate distance was set to 4.5 cm along the direction normal to the target. During deposition, the ZnMgO:Ga films were deposited on the Al_2O_3 at a deposition temperature of 400 °C. Both ultra pure (99.999%) oxygen and argon gas were introduced into the chamber (base pressure $< 1 \times 10^{-7}$ Torr) using mass-flow controllers. The partial pressure of oxygen and argon are 1×10^{-5} Torr and 1×10^{-3} Torr respectively, which were calculated as the total gas pressure read from the ion gauge times the proportion of the O_2 or Ar gas in the total pressure read from the RGA, which was mounted on the chamber. All films were grown for 10 000 pulses, which gave a thickness ≈190 nm. After deposition, the heater was cooled to room temperature at 5 °C min^{-1}. More experimental details can be found in the literature.[14]

Film Characterization: Film carrier concentration, mobility and conductivity as a function of temperature were determined using a Lakeshore Hall effect measurement system in the van-der-Pauw geometry with indium contacts soldered to the sample. Conductivities were confirmed using the collinear four-point-probe technique. The Mg to Zn ratio in targets and films was determined using energy dispersive X-ray analysis (EDX, Princeton Gamma-Tech Prism) and confirmed using inductively coupled plasma atomic emission spectroscopy (ICP-AES). The Ga to Zn ratio was measured using X-ray fluorescence (XRF) performed on a Matrix Metrologies MaXXi 5 system. A Philips (FEI) CM200 TEMA TEM system was used to obtain HRTEM and SADP images, while a Titan TEM/STEM (FEI) was used to obtain EDS-STEM images. The crystal structure was characterized using a Rigaku Ultima IV XRD system with Cu Ka radiation. The thickness of the sample was measured using a Veeco Dektak8 Advanced development Profiler.

Supporting Information

Supporting Information is available from the Wiley Online Library or from the author.

Acknowledgements

This work was supported through the SunShot Initiative funded by the U.S. Department of Energy, Office of Energy Efficiency and Renewable Energy, Office of Solar Energy Technology under Award Number DE-AC36–08GO28308 to NREL. The authors thank Prof. Brian Gorman for TEM and SADP measurements, along with Dr. Paul Kotula for HRSTEM and EDS measurements. The authors also thank Dr. Paul Ndione, Dr. Ajaya Sidgel, and Dr. Robert Pasquarelli for assistance and helpful discussions.

Received: September 16, 2013
Revised: November 18, 2013
Published online: January 30, 2014

[1] A. Ohtomo, M. Kawasaki, T. Koida, K. Masubuchi, H. Koinuma, Y. Sakurai, Y. Yoshida, T. Yasuda, Y. Segawa, *Appl. Phys. Lett.* **1998**, *72*, 2466.
[2] K. Matsubara, H. Tampo, H. Shibata, A. Yamada, P. Fons, K. Iwata, S. Niki, *Appl. Phys. Lett.* **2004**, *85*, 1374.
[3] D. Cohen, K. Ruthe, S. Barnett, *J. Appl. Phys.* **2004**.
[4] W. Wei, C. Jin, J. Narayan, R. J. Narayan, *J. Appl. Phys.* **2010**, *107*, 013510.

[5] W. Yang, R. Vispute, S. Choopun, R. Sharma, T. Venkatesan, H. Shen, *Appl. Phys. Lett.* **2001**, *78*, 2787.
[6] D. Cohen, S. Barnett, *J. Appl. Phys.* **2005**, *98*, 053705.
[7] M. Brandt, H. Von Wenckstern, M. Stölzel, H. Hochmuth, M. Lorenz, M. Grundmann, *Semicond. Sci. Technol.* **2010**, *26*, 014040.
[8] T. Minemoto, T. Minemoto, Y. Hashimoto, Y. Hashimoto, T. Satoh, T. Satoh, T. Negami, T. Negami, H. Takakura, H. Takakura, Y. Hamakawa, Y. Hamakawa, *J. Appl. Phys.* **2001**, *89*, 8327.
[9] X. Li, A. Kanevce, J. V. Li, I. Repins, *Phys. Status Solidi C* **2010**, *7*, 1703.
[10] D. Olson, S. Shaheen, M. White, W. Mitchell, M. van Hest, R. Collins, D. Ginley, *Adv. Funct. Mater.* **2006**, *17*, 264.
[11] K. Knutsen, R. Schifano, E. Marstein, *Phys. Status Solidi A* **2012**.
[12] T. Gershon, K. Musselman, A. Marin, R. Friend, J. MacManus-Driscoll, *Sol. Energy Mater. Sol. Cells* **2012**, *96*, 148.
[13] K. Koike, K. Hama, I. Nakashima, S. Sasa, M. Inoue, M. Yano, *Jpn. J. Appl. Phys.* **2005**, *44*, 3822.
[14] Y. Ke, J. J. Berry, P. Parilla, A. Zakutayev, R. P. O'hayre, D. Ginley, *Thin Solid Films* **2012**, *520*, 3697.
[15] X. Gu, L. Zhu, Z. Ye, Q. Ma, H. He, Y. Zhang, B. Zhao, *Sol. Energy Mater. Sol. Cells* **2008**, *92*, 343.
[16] K. Maejima, H. Shibata, H. Tampo, K. Matsubara, S. Niki, *Thin Solid Films* **2010**, *518*, 2949.
[17] H. Agura, A. Suzuki, T. Matsushita, T. Aoki, M. Okuda, *Thin Solid Films* **2003**, *445*, 263.
[18] T. Minami, *Semicond. Sci. Technol.* **2005**, *20*, S35.
[19] D. C. Look, T. C. Droubay, S. A. Chambers, *Appl. Phys. Lett.* **2012**, *101*, 102101.
[20] J. Lu, S. Fujita, T. Kawaharamura, H. Nishinaka, Y. Kamada, T. Ohshima, *Appl. Phys. Lett.* **2006**, *89*, 262107/1.
[21] K. Fleischer, E. Arca, C. Smith, I. Shvets, *Appl. Phys. Lett.* **2012**, *101*, 121918.
[22] Q. Ma, H. He, Z. Ye, L. Zhu, J. Huang, Y. Zhang, B. Zhao, *J. Solid State Chem.* **2008**, *181*, 525.
[23] A. Bikowski, K. Ellmer, *J. Appl. Phys.* **2013**, *114*, 063709.
[24] A. Janotti, C. G. Van de Walle, *Phys. Rev. B* **2007**, *76*, 165202.
[25] S. Lany, A. Zunger, *Phys. Rev. Lett.* **2007**, *98*, 045501.
[26] D. Demchenko, B. Earles, H. Liu, V. Avrutin, N. Izyumskaya, Ü. Özgür, H. Morkoç, *Phys. Rev. B* **2011**, *84*, 075201.
[27] F. Tuomisto, V. Ranki, K. Saarinen, D. C. Look, *Phys. Rev. Lett.* **2003**, *91*, 205502.
[28] D. C. Look, K. Leedy, L. Vines, B. Svensson, A. Zubiaga, F. Tuomisto, D. Doutt, L. Brillson, *Phys. Rev. B* **2011**, *84*, 115202.
[29] J. T-Thienprasert, S. Rujirawat, W. Klysubun, J. Duenow, T. Coutts, S. Zhang, D. C. Look, S. Limpijumnong, *Phys. Rev. Lett.* **2013**, *110*, 055502.
[30] S. Lany, A. Zunger, *Phys. Rev. B* **2008**, *78*, 235104.
[31] C. Bundesmann, A. Rahm, M. Lorenz, M. Grundmann, M. Schubert, *J. Appl. Phys.* **2006**, *99*, 113504.
[32] L. Hedin, *Phys. Rev.* **1965**, *139*, A796.
[33] M. Shishkin, M. Marsman, G. Kresse, *Phys. Rev. Lett.* **2007**, *99*, 246403.
[34] S. Lany, H. Raebiger, A. Zunger, *Phys. Rev. B* **2008**, *77*, 241201.
[35] A. Schleife, C. Rödl, J. Furthmüller, F. Bechstedt, *New J. Phys.* **2011**, *13*, 085012.
[36] K. Ellmer, in Transparent Conductive Zinc Oxide: Basics and Applications in Thin Film Solar Cells, Vol. *104* (Eds: K. Ellmer, A. Klein, B. Rech), Springer-Verlag, Berlin Heidelberg **2008**, 35.
[37] N. Chen, C. Sui, *Mater. Sci. Eng., B* **2006**, *126*, 16.
[38] R. L. Weiher, *Phys. Rev.* **1966**, *152*, 736.
[39] N. Ashkenov, B. Mbenkum, C. Bundesmann, V. Riede, M. Lorenz, D. Spemann, E. Kaidashev, A. Kasic, M. Schubert, M. Grundmann, *J. Appl. Phys.* **2003**, *93*, 126.
[40] S. T. Pantelides, *Rev. Modern Phys.* **1978**, *50*, 797.
[41] B. K. Meyer, J. Sann, D. M. Hofmann, C. Neumann, A. Zeuner, *Semicond. Sci. Technol.* **2005**, *20*, S62.
[42] H. Peng, D. O. Scanlon, V. Stevanovic, J. Vidal, G. W. Watson, S. Lany, *Phys. Rev. B* **2013**, *88*, 115201.
[43] A. Zakutayev, N. H. Perry, T. O. Mason, D. S. Ginley, S. Lany, *Appl. Phys. Lett.* **2013**, *103*, 232106.
[44] L. Makowski, M. Glicksman, *J. Phys. Chem. Solids* **1973**, *34*, 487.
[45] F. A. Kröger, The Chemistry of Imperfect Crystals North-Holland, Amsterdam **1974**.
[46] D. Wegner, E. A. Meyer, *J. Phys.: Condens. Matter* **1989**, *1*, 5403.
[47] S. Lany, V. Ostheimer, H. Wolf, T. Wichert, *Phys. B* **2001**, *958*, 308.
[48] G.-Y. Huang, C.-Y. Wang, J.-T. Wang, *J. Appl. Phys.* **2009**, *105*, 073504.
[49] P. Erhart, K. Albe, *Appl. Phys. Lett.* **2006**, *88*, 201918.
[50] K. Ellmer, A. Klein, B. Rech, *Springer Series Mater. Sci.* **2007**, *104*, 1.
[51] H. Liu, V. Avrutin, N. Izyumskaya, U. Özgür, A. B. Yankovich, *J. Appl. Phys.* **2012**, *111*, 103713.
[52] G. Kresse, D. Joubert, *Phys. Rev. B* **1999**, *59*, 1758.
[53] P. E. Blöchl, *Phys. Rev. B* **1994**, *50*, 17953.
[54] J. P. Perdew, K. Burke, M. Ernzerhof, *Phys. Rev. Lett.* **1996**, *77*, 3865.
[55] S. Lany, P. Graf, M. d'Avezac, A. Zunger, *B. Am. Phys. Soc.* **2011**, *H18*, 10.
[56] S. Lany, A. Zunger, *Model. Simul. Sci. Eng.* **2009**, *17*, 084002.
[57] M. Gajdoš, K. Hummer, G. Kresse, J. Furthmüller, F. Bechstedt, *Phys. Rev. B* **2006**, *73*, 045112.